Journal of Magnetic Resonance 311 (2020) 106680

Contents lists available at ScienceDirect

Journal of Magnetic Resonance

journal homepage: www.elsevier.com/locate/jmr

Sensitivity boosts by the CPMAS CryoProbe for challenging biological assemblies

Alia Hassan [a,*], Caitlin M. Quinn [b], Jochem Struppe [c], Ivan V. Sergeyev [c], Chunting Zhang [b], Changmiao Guo [b], Brent Runge [b,d], Theint Theint [e], Hanh H. Dao [e], Christopher P. Jaroniec [e], Mélanie Berbon [f], Alons Lends [f], Birgit Habenstein [f], Antoine Loquet [f], Rainer Kuemmerle [a], Barbara Perrone [a,*], Angela M. Gronenborn [d,g,*], Tatyana Polenova [b,d,*]

[a] Bruker Biospin Corporation, Fällanden, Switzerland
[b] Department of Chemistry and Biochemistry, University of Delaware, Newark, DE, United States
[c] Bruker Biospin Corporation, 15 Fortune Drive, Billerica, MA, United States
[d] Pittsburgh Center for HIV Protein Interactions, University of Pittsburgh School of Medicine, Pittsburgh, PA, United States
[e] Department of Chemistry and Biochemistry, The Ohio State University, Columbus, OH 43210, United States
[f] CNRS, CBMN, UMR5248, University of Bordeaux, F-33600 Pessac, France
[g] Department of Structural Biology, University of Pittsburgh School of Medicine, 3501 Fifth Ave., Pittsburgh, PA, United States

ARTICLE INFO

Article history:
Received 25 September 2019
Revised 19 December 2019
Accepted 21 December 2019
Available online 23 December 2019

Keywords:
MAS NMR
CryoProbe
Magic angle spinning
Biological assemblies

ABSTRACT

Despite breakthroughs in MAS NMR hardware and experimental methodologies, sensitivity remains a major challenge for large and complex biological systems. Here, we report that 3–4 fold higher sensitivities can be obtained in heteronuclear-detected experiments, using a novel HCN CPMAS probe, where the sample coil and the electronics operate at cryogenic temperatures, while the sample is maintained at ambient temperatures (BioSolids CryoProbe™). Such intensity enhancements permit recording 2D and 3D experiments that are otherwise time-prohibitive, such as 2D ^{15}N-^{15}N proton-driven spin diffusion and ^{15}N-^{13}C double cross polarization to natural abundance carbon experiments. The benefits of CPMAS CryoProbe-based experiments are illustrated for assemblies of kinesin Kif5b with microtubules, HIV-1 capsid protein assemblies, and fibrils of human Y145Stop and fungal HET-s prion proteins – demanding systems for conventional MAS solid-state NMR and excellent reference systems in terms of spectral quality. We envision that this probe technology will be beneficial for a wide range of applications, especially for biological systems suffering from low intrinsic sensitivity and at physiological temperatures.

1. Introduction

During the past decade, the field of structural biology has undergone a revolution. Thanks to the transformative advances in instrumentation for cryoelectron microscopy (cryo-EM) and NMR spectroscopy, structures of complex biological systems are now accessible at atomic-level resolution [1]. The advent of high-field magnets (fields above 18.8 T), digital radio frequency (rf) consoles, and breakthroughs in magic angle spinning (MAS) probe technologies opened new avenues in the field of biological solid-state NMR. Multidimensional NMR experiments are now performed on large biomolecules and assemblies for atomic-level structural and dynamic characterization [2,3], previously out of reach for any structural biology technique.

One particularly impressive and rapidly growing area is high-speed MAS NMR spectroscopy (MAS frequencies of 100–150 kHz) combined with ^{1}H detection, yielding spectra of unprecedented high resolution (^{1}H line widths of several Hz), with small amounts of sample (only tens of nanomoles) and short experiment times [4–8]. High-speed MAS NMR experiments work best for highly concentrated and/or dense samples, whereas for low concentration samples the experimental choices are limited. Examples of such samples are proteins bound to cytoskeleton (microtubules, actin) filaments [9,10] or membrane proteins embedded in cellular extracts, where only a small fraction of the sample is isotopically labeled [11].

* Corresponding authors.
E-mail addresses: Alia.Hassan@bruker.com (A. Hassan), barbara.perrone@bruker.com (B. Perrone), amg100@pitt.edu (A.M. Gronenborn), tpolenov@udel.edu (T. Polenova).

https://doi.org/10.1016/j.jmr.2019.106680
1090-7807/

In general, with the conventional MAS NMR probes operating at room temperature, and regardless of probe design, the sensitivity ceiling is rapidly reached, with sensitivity remaining the major challenge in biosolids NMR. Here, we address this challenge by using cryogenically cooled MAS probes, where the sample coil and the electronics operate at cryogenic temperatures, while the sample is maintained at ambient temperature. While this technology is mature for solution NMR applications, it has not been commercially available for triple resonance MAS NMR experiments until very recently, with the introduction of the Bruker CPMAS CryoProbe.

We present results, demonstrating that 3 to 4- fold sensitivity enhancements are obtained in heteronuclear-detected experiments of insoluble and non-crystalline biological assemblies, using a novel CPMAS cryoprobe. The selected systems are challenging to study with conventional room-temperature MAS NMR probes, due to their low intrinsic sensitivity which renders multidimensional experiments time prohibitive: a sample of U-^{13}C,^{15}N-Kif5b kinesin bound to microtubules in which the weight fraction of isotopically labeled protein is only 9% (Fig. 1a) and a sample containing conical assemblies of HIV-1 U-^{15}N capsid protein without ^{13}C labels (Fig. 1b). Furthermore, the large sensitivity enhancements afforded by the CPMAS CryoProbe also permit detailed characterization of tubular assemblies of HIV-1 U-^{13}C,^{15}N capsid protein (Fig. 1c) and fibrils of human Y145Stop and fungal HET-s prion proteins (Fig. 1d and e).

Single-scan 2D ^{13}C-^{13}C correlation spectra and high-quality 2D and 3D homo- and heteronuclear ^{13}C-detected spectra were recorded on all systems at 14.1 T with the CPMAS CryoProbe in remarkably short experimental time. Multidimensional data of this sort are otherwise inaccessible for such complex systems, even at high magnetic fields. Data sets acquired with the CPMAS CryoProbe contain signals that otherwise are not detectable, aiding in resonance assignment. Most remarkably, 2D ^{15}N-^{13}C NCO and NCA spectra were recorded for the tubular assembly of HIV-1 U-^{15}N-labeled CA, containing natural abundance carbon atoms. An analysis of the sensitivity and resolution in these data sets is presented here.

Overall, the benefits of the CPMAS CryoProbe for atomic-resolution characterization of large biological assemblies of low intrinsic sensitivity will further push the boundaries of MAS NMR in the biological arena.

2. Materials and methods

2.1. Materials

Common chemicals were purchased from Fisher Scientific or Sigma-Aldrich. Porcine brain tubulin, GTP and paclitaxel were purchased from Cytoskeleton, Inc. $^{15}NH_4Cl$ and U-$^{13}C_6$ glucose were purchased from Cambridge Laboratories, Inc. EDTA-free protease inhibitor tablets were obtained from Roche. Chromatography columns were purchased from GE Healthcare. The 400 mesh copper grids coated with formvar and stabilized with evaporated carbon films were purchased from Electron Microscopy Science.

2.2. NMR sample preparation

Kif5b/MT assemblies were prepared following a protocol developed earlier for the preparation of CAP-Gly/MT assemblies [9]. The human Kif5b motor domain construct (residues 1–349) was prepared using the pET28b vector fused with a His_6-SMT3 Tag at the N-terminus (in the form of His_6-SMT3-Kif5b). *E. coli* BL21(DE3) cells were transformed with the His_6-SMT3-Kif5b encoding vector. The His_6-Ulp1 protease construct was provided by Dr. Christopher Lima from Weill Medical College at Cornell University. For U-^{13}C,^{15}N-labeled Kif5b protein, cells were grown in 20 mL of Luria-Bertani (LB) medium containing 30 mg/L kanamycin for 6-8 hrs at 37 °C to an OD of 1.2-1.6. Following centrifugation at 4000 *g* for 5 min 4 °C, cell pellets were resuspended in 50 mL of M9 medium, containing 2 g/L $^{15}NH_4Cl$ and 4 g/L U-$^{13}C_6$-glucose and grown at 37 °C overnight. The overnight culture was transferred to 1 L of M9 medium to an OD of 0.1–0.2. Cells were grown at 37 °C to an OD of 0.6-0.8, induced with 0.8 mM IPTG, and protein was expressed at 37 °C for 4 h. Cells were harvested by centrifugation at 4000 *g* for 30 min at 4 °C, resuspended in 40 mL of PBS buffer

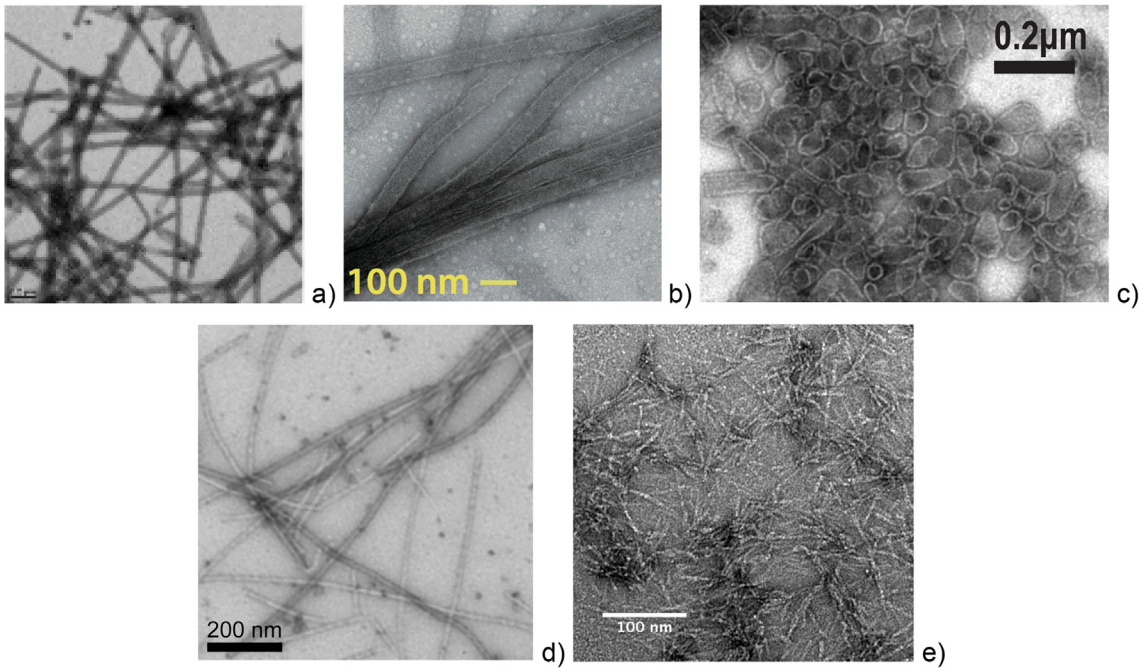

Fig. 1. TEM images of biological assemblies investigated in this report. a) U-^{13}C,^{15}N-Kif5b/microtubule assembly; b) HIV-1 U-^{15}N-CA tubular assembly; c) HIV-1 U-^{13}C,^{15}N -CA conical assembly; d) PrP23-144 fibrils; e) Het-s (218–289) fibrils.

(pH 7.4, 10 mM Na_2HPO_4, 2 mM KH_2PO_4, 137 mM NaCl, 2.7 mM KCl, 1 mM DTT), and sonicated for 20 min (10 s on and 10 s off) in an ice bath. Cell debris was removed by centrifugation at 27,000 *g* for 30 min at 4 °C. The supernatant was filtered through a 0.2 mm filter, and loaded onto a HisTrap Ni-affinity column (5 mL, GE Healthcare). The protein was eluted with a 120-240 mM imidazole concentration gradient in PBS buffer (pH 7.4, 10 mM Na_2HPO_4, 2 mM KH_2PO_4, 137 mM NaCl, 2.7 mM KCl, 1 mM DTT). Fractions containing the target protein were pooled, and the His_6-SMT3-fused U-^{13}C,^{15}N-enriched Kif5b was digested with the His_6-Ulp-1 enzyme at 4 °C overnight, to cleave off the His_6-SMT3 tag. The resulting solution was loaded on a HisTrap Ni-affinity column (5 mL, GE Healthcare). The protein was eluted with 80 mM imidazole in PBS buffer (pH 7.4, 10 mM Na_2HPO_4, 2 mM KH_2PO_4, 137 mM NaCl, 2.7 mM KCl, 1 mM DTT). The Kif5b fractions were combined and exchanged into 25 mM PIPES buffer (pH 6.8, 1 mM EGTA, 1 mM $MgCl_2$, 100 mM KCl, 1 mM DTT). The resulting solution containing pure Kif5b was concentrated to 8-10 mg/mL. For the preparation of polymerized microtubules, 18 mg of porcine brain tubulins were dissolved in 80 mM PIPES buffer (pH 6.8, 1 mM $MgCl_2$, 1 mM EGTA), and the solution was pre-cleared by ultracentrifugation at 435,400 *g* at 4 °C for 10 min. The tubulin supernatant was incubated with 20-25 μM paclitaxel and an equal volume of 80 mM PIPES polymerization mix buffer (pH 6.8, 2 mM GTP, 20% (v/v) DMSO) for 30 min at 37 °C. The polymerized microtubules were ultracentrifuged at 108,900 *g* at 20 °C for 10 min. To prepare the Kif5b/MTs assemblies, the pellets containing paclitaxel-stabilized microtubules were resuspended gently into the concentrated Kif5b solution to a 2:1 molar ratio of Kif5b:tubulin dimer, and the mixture was incubated at 25 °C for 45 min. The resulting complex was pelleted by ultracentrifugation at 156,800 *g* at 20 °C for 30-60 min.

For MAS NMR experiments using a Bruker EFree 3.2 mm HCN probe, the hydrated pellet of U-^{13}C,^{15}N-enriched Kif5b/MT assemblies (55 mg total weight, corresponding to ~5 mg of U-^{13}C,^{15}N-enriched Kif5b) was transferred into a thin-wall 3.2 mm Bruker rotor. For MAS NMR experiments with the CPMAS CryoProbe, the hydrated pellet of U-^{13}C,^{15}N-enriched Kif5b/MT assemblies (82.4 mg total weight, corresponding to ~7.5 mg of U-^{13}C,^{15}N-enriched Kif5b) was transferred into a thin-wall 3.2 mm Bruker CPMAS CryoProbe rotor.

HIV-1 CA protein expression, purification, and NMR sample preparation were performed as reported previously with modifications [12]. For U-^{15}N and U-^{13}C,^{15}N-labeled CA NL4-3 protein, cells were cultured in 10 mL of Luria-Bertani (LB) medium and grown at 37 °C to an OD of 1.0–1.5 OD. Following centrifugation at 4000 g for 30 min at 4 °C, cell pellets were resuspended in 100 mL of M9 medium, containing 2 g/L $^{15}NH_4Cl$ (for U-^{15}N-labeled protein), or 2 g/L $^{15}NH_4Cl$ and 2 g/L U-$^{13}C_6$-glucose (U-^{13}C,^{15}N-labeled protein) and grown at 37 °C overnight. The 100 mL overnight culture was transferred to 1 L of M9 medium to an OD of 0.10–0.15. Cells were grown at 37 °C to an OD of 1.0–1.2, induced with 0.5 mM IPTG and protein was expressed at 18 °C for 18 h. Cells were harvested by centrifugation at 4000 g for 30 min at 4 °C, resuspended in 25 mM sodium phosphate buffer (pH 7.0), and sonicated for 20 min (10 s on and 10 s off) in an ice bath. Cell debris was removed by centrifugation at 27,000*g* for 1 h at 4 °C. The pH of the supernatant was adjusted to 5.8 with acetic acid, and the conductivity was adjusted to below 2.5 ms/cm by dilution, followed by an additional centrifugation at 27,000*g* at 4 °C for 1 h. The final supernatant was loaded onto a cation exchange column (HiTrap SP HP 5 mL, GE Healthcare), and the protein was eluted with a 0–1 M NaCl gradient in 25 mM sodium phosphate buffer (pH 5.8), 1 mM DTT, 0.02% NaN_3. Fractions containing CA protein were pooled and further purified by gel filtration using a size-exclusion column (HiLoad 26/600 Superdex 75 prep grade, GE Healthcare), equilibrated with 25 mM sodium phosphate buffer (pH 5.5), 1 mM DTT, 0.02% NaN_3. Fractions containing CA protein were combined and concentrated to 20–30 mg/mL.

Tubular assemblies of U-^{15}N CA protein were prepared from 30 mg/mL protein solution in 25 mM phosphate buffer (pH 5.5) containing 400 mM NaCl. The solution was incubated at 37 °C for 1 h and stored at 4 °C for subsequent NMR experiments.

Conical assemblies of U-^{13}C,^{15}N-labeled CA NL4-3 protein were prepared from 30 mg/mL protein solution in 50 mM MES buffer (pH 6.0) containing 150 mM NaCl and 0.9 mM IP6. The solution was incubated at 25 °C for 1 h and stored at 4 °C for subsequent NMR experiments.

The final CA assemblies were pelleted by centrifugation at 10,000*g*, 4 °C, for 15 min in a Beckmann ultracentrifuge, the supernatant was removed, and 87 mg of these assemblies, corresponding to ~65 mg of U-^{13}C,^{15}N- or U-^{15}N-labeled CA, were packed into 3.2 mm Bruker CPMAS CryoProbe rotors.

Human Y145Stop PrP fibrils: Uniformly ^{13}C and ^{15}N enriched human Y145Stop prion protein (huPrP23-144) was expressed and purified as described in detail in previous reports [13–15]. Amyloid fibrils were prepared by dissolving purified lyophilized protein in ultrapure water at a concentration of 400 μM (~5 mg/mL), followed by the addition of 1.0 M potassium phosphate buffer (pH 6.4), to a final concentration of 50 mM and incubation at 25 °C under quiescent conditions for 48 h [14,15]. Fibrils were washed with several aliquots of 50 mM potassium phosphate buffer (pH 6.4), containing 0.02% (v/v) sodium azide and ~25 mg of the fibrils were transferred to a 3.2 mm Bruker CPMAS CryoProbe rotor via centrifugation.

HET-S fibrils: *E. coli* strain BL21(DE3) pLysS was transformed with pET21-HET-s(218–289)-His6 vector and plated onto LB agar plates containing 100 μg/mL Ampicillin. As initial culture, 5 mL LB/Amp medium was inoculated with a single colony and incubated at 37 °C under shaking until exponential growth phase (OD_{600} = 0.7). Cells from the fresh initial LB culture were harvested by centrifugation (1000*g*, 10 min), added to 100 mL labeled M9 medium and grown overnight at 37 °C. This culture was used to inoculate 1 L of labeled medium at OD_{600} = 0.2, grown at 37 °C, to OD_{600} = 0.8 and expression was induced with 0.75 mM IPTG for 4 h. Protein expression was carried out in M9 minimal medium supplemented with 1 g/L of ^{15}NH4Cl and 2 g/L of ^{13}C glucose as nitrogen and carbon sources. Cells were harvested by centrifugation (6000*g*, 30 min, 4 °C) and frozen (−80 °C) until purification. Frozen cells pellets were thawed and lyzed by sonication on ice in 25 mL buffer A1 (Tris 50 mM, 150 mM NaCl, pH 8). Protein inclusion bodies and cell debris was collected by centrifugation (15,000*g*, 1h, 4 °C) and the cell pellet was shaked vigorously at 37 °C for 20 min in 20 mL of buffer A1, supplemented with 2% Triton X-100, centrifuged (50,000*g*, 10 min, 4 °C), washed with buffer A1 (2 h, 37 °C), centrifuged (50,000*g*, 10 min, 4 °C) and resuspended in 10 mL of extraction buffer (50 mM Tris, 0.5 M NaCl, 6 M Gu-HCl pH 8). The suspension was incubated overnight at 60 °C, sonicated and ultra-centrifuged (250,000*g*, 1 h, 25 °C) before column purification. Protein was applied to a 5 mL Histrap HP column (GE Healthcare), previously equilibrated with buffer A2 (50 mM Tris, 0.5 M NaCl, 20 mM imidazole, 8 M urea, pH 8), and eluted with buffer B (50 mM Tris, 0.5 M NaCl, 500 mM imidazole, 7 M urea, pH 8). Protein fractions were monitored by UV absorbance at 280 nm and 214 nm. Protein containing fractions were pooled and buffer exchanged into 150 mM acetic acid pH 3.0, over a HiPrep 26/10 desalting column (GE Healthcare) and fractions were analyzed on 12% Tris-tricine SDS-PAGE. 12% (v/v) of 3 M Tris-HCl, pH 8 was added to a pure solution of 0.1 mM of HET-s (218–289) in 150 mM acetic acid, to adjust the pH to 7. Self-assembly was promoted by agitation at RT for several days.

2.3. Transmission electron microscopy (TEM)

The morphology of Kif5b/MT and HIV-1 CA assemblies was characterized by transmission electron microscopy (TEM). TEM analysis of the CA assemblies was performed with a Zeiss Libra 120 transmission electron microscope operating at 120 kV. Samples were negatively stained with uranyl acetate (2% w/v), deposited onto 400 mesh, formvar/carbon-coated copper grids, and air dried for 40–45 min. The copper grids were glow discharged prior to staining, so that the assemblies are uniformly spread on the grid surface and adhere to it. Analogous negative stain TEM analysis for huPrP23-144 fibrils was performed for huPrP23-144 fibrils with a FEI Techai G2 Spirit TEM instrument operating at 80 kV.

For the HET-s sample, TEM analysis was performed with a FEI CM120 microscope at 120 kV with a Gatan USC1000 2 k × 2 k camera. The sample was prepared using a droplet of Het-s fibrils, diluted in 150 mM acetic acid buffer, and applied to glow-discharged 300 mesh carbon-coated copper grids for 1 min, washed with water, stained with 2% uranyl acetate (w/v) for 1 min and dried under dark condition.

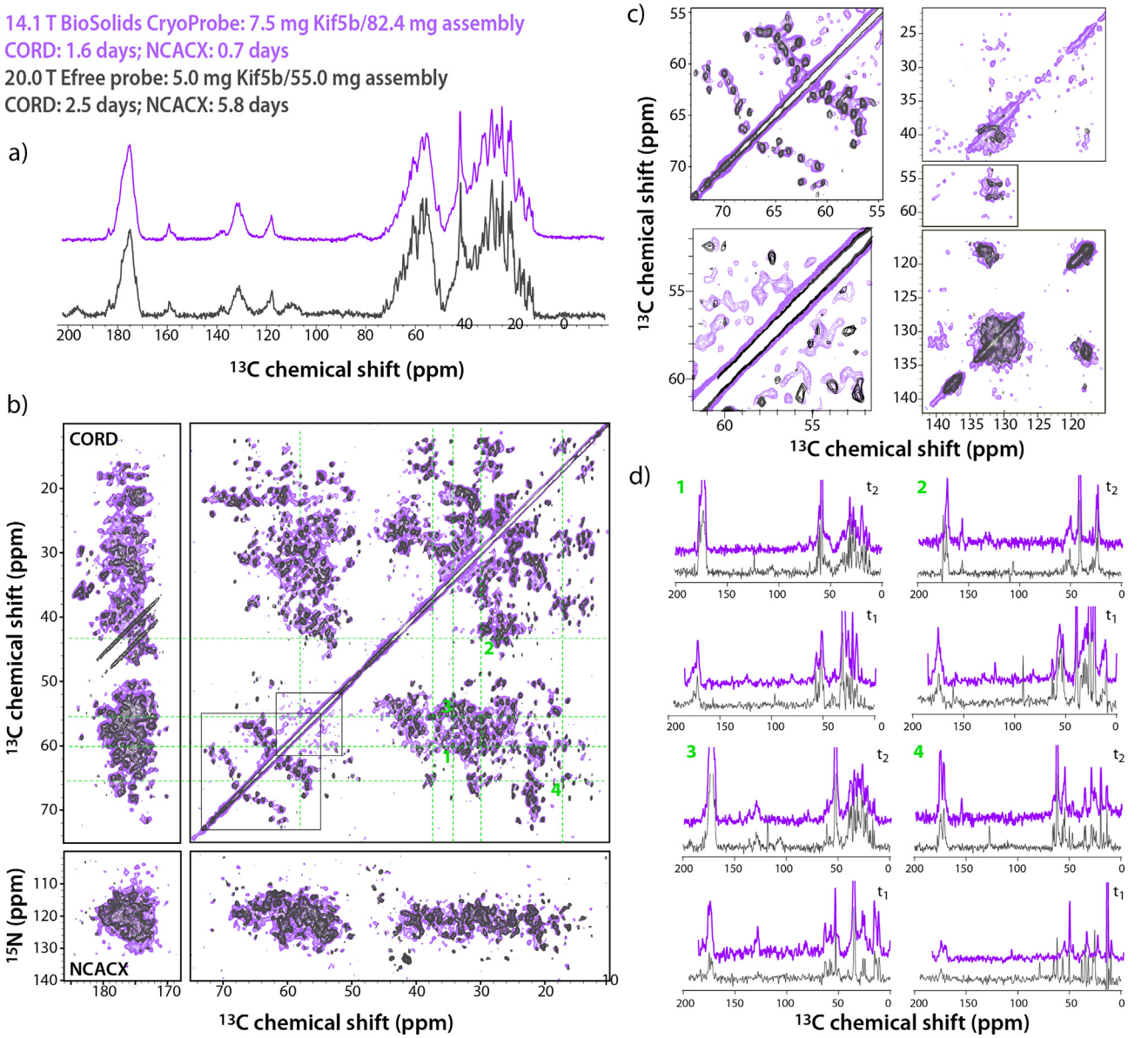

Fig. 2. a) and b) 1D and 2D MAS NMR spectra of Kif5b/MT assembly acquired with the 3.2 mm CPMAS CryoProbe at 14.1 T (purple) and 3.2 mm EFree probe at 20.0 T (black): a) ^{13}C CPMAS; b) CORD (top) and NCACX (bottom). c) Expansions of the CORD spectra showing selected regions, containing the aliphatic and aromatic sidechain correlations. d) Selected 1D traces through the direct (top) and indirect (bottom) dimensions of the CORD spectrum at the frequencies indicated by green dashed lines. The CPMAS spectra were collected with 64 and 512 scans, and the total acquisition time was 16 ms. The SNR was 135 and 136; the effective SNR per mg of protein per square root of scan and corrected for the B_0 was 2.2 and 0.7 for CPMAS CryoProbe and EFree probe spectra, respectively. The CORD spectra were collected with 36 and 192 scans, the recycle delays were 2 and 3 s; the total experiment times were 1.6 and 2.5 days. The SNR (1st FID) was 60 and 59 with equivalent processing. The effective SNR per mg of protein per square root of scan and corrected for the B_0 was 1.3 and 0.5 for CPMAS CryoProbe and EFree probe spectra, respectively. The NCACX spectra were collected with 256 and 3072 scans, the recycle delays were 3 and 2 s; the total experiment times were 17 and 139 h. The SNR (1st FID) was 13 for both data sets. The effective SNR per mg of protein per square root of scan and corrected for the B_0 was 0.1 and 0.02 for CPMAS CryoProbe and EFree probe spectra, respectively. The MAS frequency in both cases was 14 kHz. The estimated amount of U-^{13}C,^{15}N-Kif5b in the samples for experiments with the CPMAS CryoProbe and EFree probe was 7.5 and 5.0 mg; the total amount of assemblies packed in the rotors was 82.4 and 55.0 mg. (For interpretation of the references to color in this figure legend, the reader is referred to the web version of this article.)

2.4. MAS NMR spectroscopy

Experiments were performed on 14.1 T narrow bore Bruker NEO or Avance III HD spectrometers outfitted with 3.2 mm CPMAS CryoProbe prototypes. Larmor frequencies were 600.3 MHz (^{1}H), 150.9 MHz (^{13}C) and 60.8 MHz (^{15}N). Sample temperatures were 10 ± 1 °C (kinesin/microtubule assemblies), 5 ± 1 °C (HIV-1 CA assemblies), 5 ± 1 °C (huPrP23-144 fibrils), and 0 ± 1 °C (HET-S fibrils), calibrated with KBr used as an external temperature standard [16] and regulated by a Bruker variable temperature controller. MAS NMR spectra were collected at frequencies of 11.000 to 14.000 ± 0.002 kHz regulated by a Bruker MAS controller. Typical 90° pulse lengths were 2.8–3.3 μs (^{1}H), 4.0–4.4 μs (^{13}C), and 5.5–6.4 μs (^{15}N). ^{1}H–^{13}C and ^{1}H-^{15}N CP was performed with a 30% linear amplitude or 20% tangential ramp on ^{1}H, with the ^{13}C/^{15}N radio frequency (rf) field of 55–60/40–45 kHz matched to Hartmann-Hahn conditions at the first spinning sideband. Typical ^{1}H–^{13}C and ^{1}H-^{15}N contact times were 0.8–1.5 ms and 1.0–2.0 ms, respectively, and dependent on the sample. Typical double CP (DCP) power levels of 17–19 or 36–38 kHz on ^{13}C and 3–5 kHz on ^{15}N were used with optimized ^{15}N-^{13}C DCP contact time of 1–6 ms. A 30% and 25% tangential amplitude ramp was applied on ^{13}C with the rf carrier frequency placed at 170–190 and 50–60 ppm in NCO and NCA transfers, respectively. TPPM or swTPPM decoupling (80–90 kHz) was applied during the evolution and acquisition periods. The CORD or DARR mixing time was 50 ms; ^{13}C–^{13}C and ^{15}N-^{15}N PDSD mixing times were 20 ms and 4 s, respectively.

Spectra of Kif5b/MT and HIV-1 CA assemblies were also acquired on a 20.0 T narrow bore Bruker AVIII spectrometer outfitted with a 3.2 mm EFree HCN probe. Larmor frequencies were 850.4 MHz (^{1}H), 213.8 MHz (^{13}C) and 86.2 MHz (^{15}N). The sample temperature was 10.0 ± 0.5 °C, calibrated with KBr used as an external temperature standard and regulated by a Bruker variable temperature controller. MAS NMR spectra were collected at a frequency of 14.000 ± 0.002 kHz regulated by a Bruker MAS controller. ^{13}C and ^{15}N chemical shifts were referenced with respect to external standards adamantine and NH_4Cl, respectively. Typical 90° pulse lengths were 2.7 μs (^{1}H), 2.9 μs (^{13}C), and 4.7 μs (^{15}N). ^{1}H–^{13}C and ^{1}H-^{15}N CP was performed with a linear amplitude ramp of 80–100%, with the ^{1}H radio frequency (rf) field of 82 kHz; the center of the ramp on the ^{13}C or/and ^{15}N channels was matched to Hartmann-Hahn conditions at the first spinning sideband. Typical ^{1}H–^{13}C and ^{1}H-^{15}N contact times were 0.8–1.1 ms and 1.2 ms, respectively. Typical DCP power levels were 30 kHz on ^{13}C and 45 kHz on ^{15}N with optimized ^{15}N-^{13}C DCP contact time of 4.5 ms. SPINAL-64 decoupling (80 kHz) was applied during the evolution and acquisition periods. The CORD mixing time was 50 ms.

2D NCA MAS NMR spectra of huPrP23-144 fibrils (~12 mg) were also recorded at a frequency of 11.111 ± 0.003 kHz and sample temperature of 5 ± 1 °C using a three-channel 500 MHz Varian spectrometer equipped with a 3.2 mm BioMAS™ probe [17] in the ^{1}H–^{13}C–^{15}N configuration.

Spectra of HET-s fibrils were also acquired on a 14.1 T UltraShield Bruker NEO spectrometer outfitted with a 3.2 mm EFree HCN probe. The sample temperature was set to 5.0 ± 1 °C, calibrated with DSS used as an internal temperature reference [18] and regulated by a Bruker variable temperature controller. MAS NMR spectra were collected at a of 16.000 ± 0.002 kHz regulated by a Bruker MAS controller. ^{13}C chemical shifts were referenced with respect to DSS. Typical 90° pulse lengths were 2.5 μs (^{1}H) and 3.0 μs (^{13}C). ^{1}H–^{13}C CP contact times was 1.2 ms. SPINAL-64

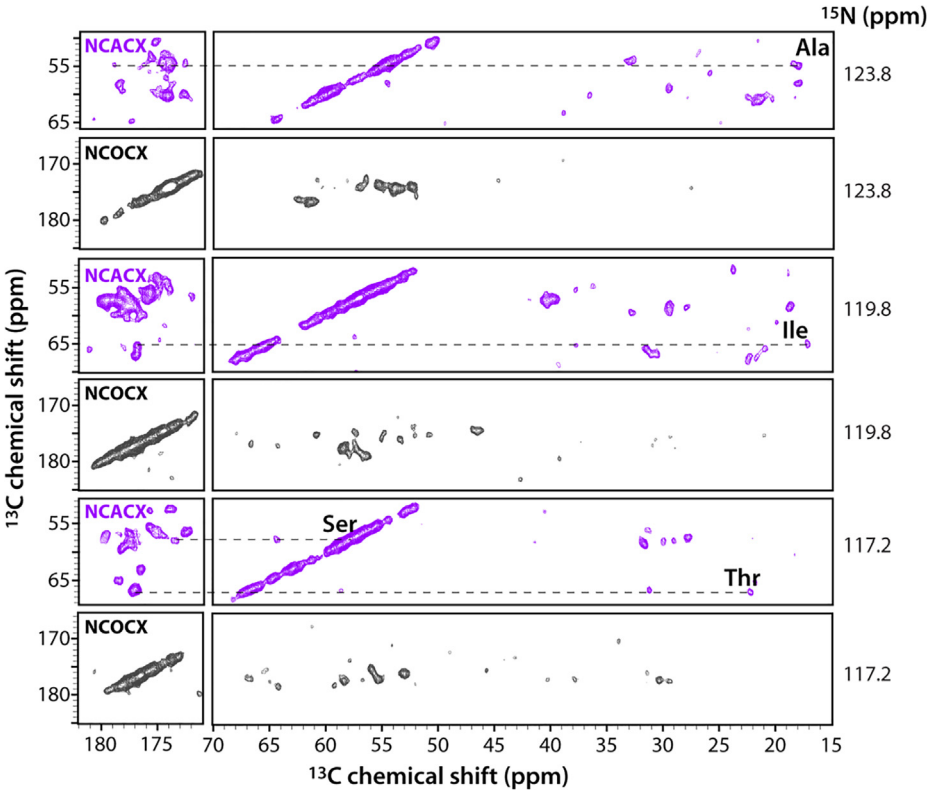

Fig. 3. Selected 2D planes for the 3D NCACX (purple) and NCOCX (black) spectra of Kif5b/MT assembly acquired with the 3.2 mm CPMAS CryoProbe at 14.1 T. The NCACX spectrum was acquired with 48 scans per FID, as 1818 × 64 × 50 ($t_3 \times t_2 \times t_1$) complex matrix. The recycle delay was 2.7 s, and the total experiment time was 4.8 days. The effective SNR per mg of protein per square root of scan was 0.14. The NCOCX spectrum was acquired with 96 scans per FID, as 1818 × 36 × 50 ($t_3 \times t_2 \times t_1$) complex matrix. The recycle delay was 3.0 s, and the total experiment time was 6 days. The effective SNR per mg of protein per square root of scan was 0.23. (For interpretation of the references to color in this figure legend, the reader is referred to the web version of this article.)

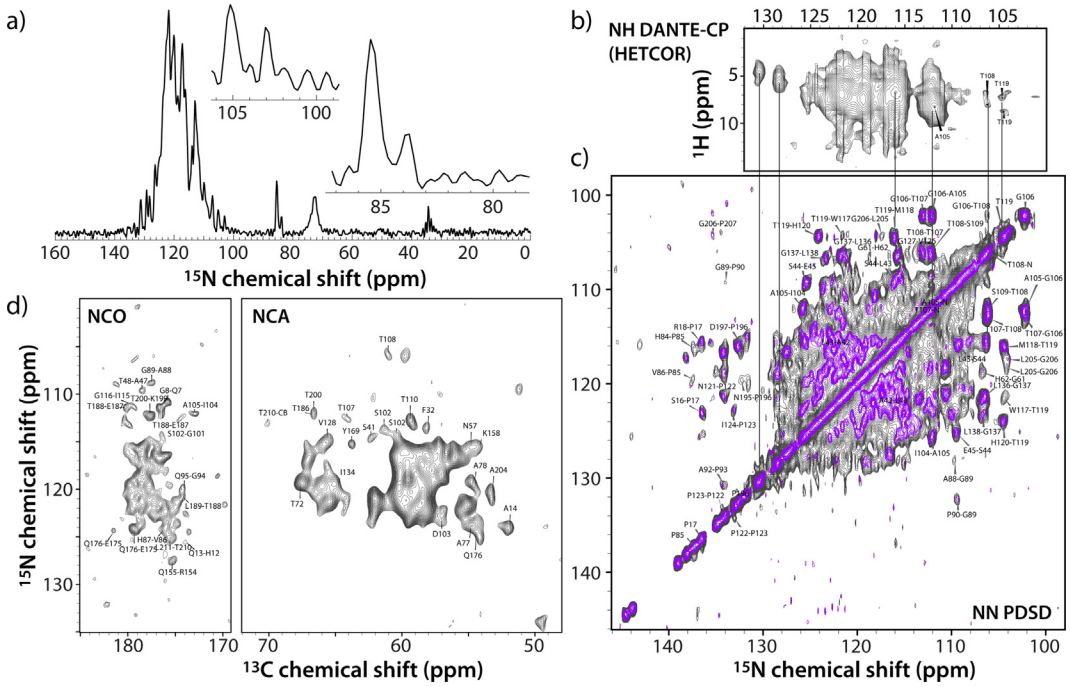

Fig. 4. 1D and 2D MAS NMR spectra of tubular assembly of U-^{15}N-CA (estimated protein amount: 65 mg) acquired with the 3.2 mm CPMAS CryoProbe: a) ^{15}N CPMAS; b) ^{1}H-^{15}N DANTE-HETCOR; c) ^{15}N-^{15}N PDSD; d) NCO (left) and NCA (right). The ^{15}N CPMAS spectrum was collected with 4 scans, the total acquisition time was 33 ms. The SNR was 59; the effective SNR per mg of protein per square root of scan was 1.3. Expansions around selected regions of the spectrum illustrate the high spectral resolution. The ^{1}H-^{15}N DANTE-HETCOR spectrum was collected with 48 scans; the total experiment time was 5.2 h. The SNR (1st FID) = 20. The ^{15}N-^{15}N PDSD spectrum was collected with 64 scans; the total experiment time was 13.75 h. The SNR (1st FID) – 128. The spectrum was processed with 90- and 60- degree shifted sinebell functions (gray and purple contours, respectively). The NCO and NCA spectra were both acquired with 512 scans, as 2048 × 54 and 2048 × 62 ($t_2 \times t_1$) complex matrices; and the total experiment time was 23.5 and 27 h, respectively. The SNR (1st FID) was 5 (NCA) and 7.6 (NCO). (For interpretation of the references to color in this figure legend, the reader is referred to the web version of this article.)

decoupling (80 kHz) was applied during the evolution and acquisition periods. The PDSD mixing time was 50 ms.

2.5. NMR data processing and analysis

Kif5b/MT and HIV-1 CA assemblies: All spectra were processed in TopSpin and NMRPipe [19] and analyzed in SPARKY [20]. For 2D CORD and 3D NCACX and NCOCX data sets, 60° or 90°-shifted sine bell apodization, followed by a Lorentzian-to Gaussian transformation was applied in all dimensions. For spectra acquired with a Bruker 3.2 mm EFree HCN probe, forward linear prediction to twice the number of the original data points was used in the indirect dimension in some data sets, followed by zero filling to twice the total number of points.

Human Y145Stop fibrils: All spectra were processed in NMRPipe and analyzed in SPARKY and nmrglue [21]. The 2D NCA data sets acquired with the CPMAS CryoProbe and BioMAS probe were processed in identical manner with 90°-shifted sine bell apodization in both dimensions. For the 2D N(CA)CX and N(CO)CX and 3D NCACX and NCOCX data sets 81°- shifted sine bell apodization was applied in all dimensions.

HET-S fibrils: All spectra were processed in TopSpin and analyzed in CCPnmr [22]. A 90°-shifted sine bell apodization was applied in all dimensions.

3. Results

3.1. Kif5b/microtubule assemblies

A comparison of 1D spectra of Kif5b/MT assemblies acquired at 14.1 T with the CPMAS CryoProbe and at 20.0 T with the EFree probe are shown in Fig. 2a. The effective signal-to-noise ratios (SNR) per mg of protein per square root of scan are 2.2 and 0.7, after correction for the different B_0 fields, which translates into a sensitivity gain of 3.1 with the CPMAS CryoProbe compared to the EFree probe. 2D CORD spectra are shown in Fig. 2b–d. The estimated sensitivity gain in the first FID with the CPMAS CryoProbe is 2.6 as compared to the EFree probe, which permitted data collection in 1.6 vs. 2.5 days. Furthermore, the high intrinsic SNR of the CPMAS CryoProbe allowed the acquisition of a single-scan CORD spectrum in 1.2 h, with a SNR of 14.1 for the 1st FID (Fig. S1, Supporting Information). The single-scan CORD spectrum is beneficial for sample quality assessment and estimating the secondary structure of the protein. From the superposition of the two 2D CORD spectra (Fig. 2b and c) it can be appreciated that many more cross peaks are present in the data recorded with the CPMAS CryoProbe. Importantly, strong correlations are observed in the aromatic region of the spectrum, a region frequently devoid of cross peaks. Likewise, an impressive 5-fold signal intensity gain is seen in the 2D NCACX spectrum (Fig. 1b). This data set was acquired in 17 h, while a data set with an equivalent SNR required 139 h of signal averaging on the 20.0 T spectrometer, equipped with the EFree probe. Such large sensitivity gains in the double-CP-based experiments exceed the nominal 3–4 fold enhancements expected from the cryogenically cooled circuit alone and they are most likely due to high B_1-homogeneity in the CPMAS CryoProbe coil design, which permits efficient heteronuclear magnetization transfers over a larger sample volume of the rf coil compared to regular solenoid rf coils.

The sensitivity enhancements are even more dramatic in 3D NCACX/NCOCX experiments. Equivalent intensity data sets recorded at 20.0 T with the EFree probe require 15 days 19 h and

19 days 8 h, respectively. Both were recorded with 25% nonuniform sampling (NUS), using random, exponentially biased NUS schedules, to take advantage of the intrinsic sensitivity gains afforded by NUS and make obtaining such spectra at all possible [23–25]. However, unfortunately, both data sets contain numerous artifacts given the inevitable issues with instrument stability for such long periods of time. In contrast, acquisition of NCACX and NCOCX spectra at 14.1 T using the CPMAS CryoProbe was achieved in a fraction of time and without NUS: 4 days 10 h and 6 days, respectively. The resulting spectra are of very high quality, both with respect to sensitivity and resolution (Fig. 3) and we anticipate accomplishing resonance assignments for the majority of residues in Kif5b based on these data sets. For the NCACX spectrum, the effective SNR in the 1st FID per mg of protein per square root of scan and corrected for the different B_0 fields are 0.14 (CPMAS CryoProbe, 14.1 T) and 0.02 (EFree probe, 20.0 T). The corresponding values for the NCOCX experiment are 0.23 and 0.03. These translate into sensitivity improvements of 7 and 7.7, respectively. If 4-fold NUS-based intrinsic sensitivity gains are factored in [23–25], the advantages of using the CPMAS CryoProbe become even more dramatic.

3.2. HIV-1 CA assemblies

We investigated two different assemblies of HIV-1 capsid protein, samples about which we have ample knowledge regarding their biophysical behavior and spectral properties.

3.2.1. U-^{15}N-CA tubular assembly

As demonstrated by us previously [12,26], this type of sample gives rise to MAS NMR spectra of excellent resolution and sensitivity. It, therefore, was selected as our test system to obtain spectra with carbon at natural abundance. 1D and 2D MAS ^{15}N cross-polarization, ^{1}H-^{15}N and ^{15}N-^{15}N correlation spectra are provided in Fig. 4b–d. The ^{1}H-^{15}N HETCOR experiment is rarely performed on fully protonated proteins at MAS frequencies below 60 kHz,

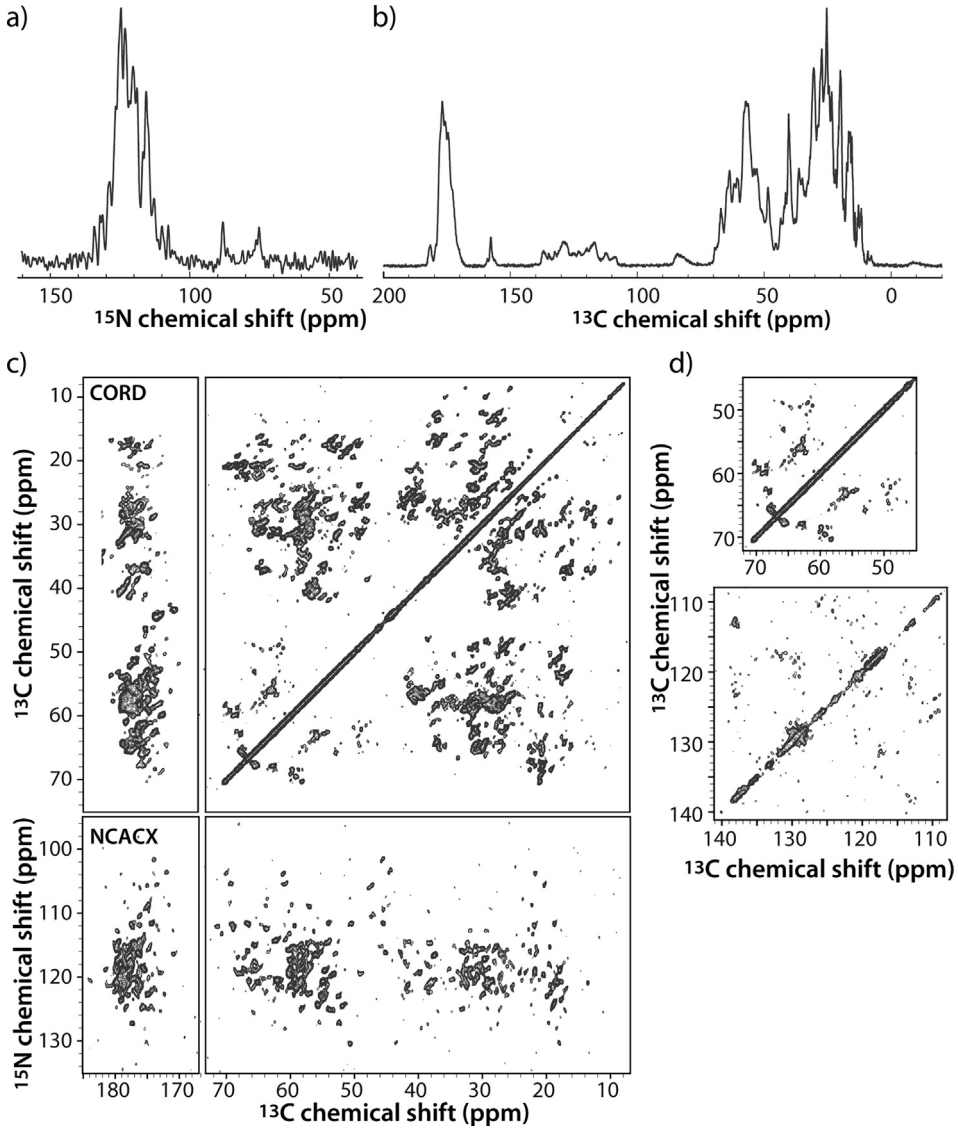

Fig. 5. 1D and 2D MAS NMR spectra of conical assembly of U-^{13}C,^{15}N-CA (estimated protein amount: 65 mg) acquired with the 3.2 mm CPMAS CryoProbe: a) and b) ^{15}N and ^{13}C CPMAS; c) CORD (top) and NCACX (bottom). d) Expansions of the CORD spectrum showing the Ser-Thr region (top) and the aromatic-to-aromatic sidechain correlations (bottom). The CPMAS spectra were collected with 4 and 8 scans, and the total acquisition time was 21 and 16 ms, respectively. The SNR was 26 and 237; the effective SNR per mg of protein per square root of scan was 0.2 and 1.0, respectively. The CORD spectrum was collected with 2 scans, the acquisition time in the direct dimension was 18 ms; the total experiment time was 1.7 h. The SNR (1st FID) was 114.7. The NCACX spectrum was collected with 40 scans, the acquisition time in the direct dimension was 17 ms; the total experiment time was 2.1 h. The MAS frequency was 14 kHz. The SNR (1st FID) was 26. The MAS frequency was 14 kHz.

and only a handful of examples of ^{15}N-^{15}N PDSD spectra of proteins exist, given the protracted experimental times associated with the necessary long PDSD mixing periods (of the order of 1–4 s). Nevertheless, the results obtained with the CPMAS CryoProbe are very encouraging. A ^{1}H frequency-swept DANTE selective excitation pulse sequence [27] followed by a short, 350-μs CP to ^{15}N for selective transfer was implemented in the ^{1}H-^{15}N HETCOR experiment (the pulse sequence is provided in Fig. S2; Supporting Information). The resulting 2D ^{1}H-^{15}N correlation spectrum is of high sensitivity with several well resolved cross peaks (Fig. 4b). Of note is also that the efficiency of the ^{1}H-^{15}N cross polarization is very high, compared with that for the conical assemblies of U-^{13}C,^{15}N-CA discussed below. Resonance assignments were easily possible by inspection, based on the known ^{15}N shifts [12] and by joint analysis with ^{15}N-^{15}N PDSD spectrum discussed below. Since the effective spectral width in the ^{1}H indirect dimension can be reduced by a factor of 3, the total experiment time decreases to 1.73 h, rendering this experiment ideally suited for incorporation as a 2D plane in a 3D experiment. In the ^{15}N-^{15}N PDSD spectrum only 64 scans were required to reach a SNR of 128 in the 1st FID. The quality of the spectrum is remarkable (Fig. 4c) with numerous well-resolved cross peaks which could be readily assigned. While many of these assignments are based on the ^{15}N shifts from our previous work [12,26], the assignments of most of the proline resonances were either ambiguous or missing, due to resonance overlap or lack of cross-peaks in the 2D and 3D NCACX/NCOCX based data sets. Gratifyingly, the present spectra contained sequential correlations to preceding and proceeding residues, which yielded unequivocal identification of all proline residues (Fig. 4c).

Perhaps most gratifying are the 2D NCO and NCA spectra (Fig. 4d). ^{15}N double cross polarization transfers to natural-abundance carbons are performed in these experiments, generally thought to be impossible to exploit in proteins. It was not only possible to record these spectra in a reasonable amount of time (23.5 h for NCA and 27 h for NCO), the quality of the data sets is such (Fig. 4d) that many resolved cross peaks were detected and readily assigned, based on available shifts for the tubular assemblies of U-^{13}C,^{15}N-CA. Overall, the set of four 2D experiments presented here, ^{1}H-^{15}N DANTE-HETCOR, ^{15}N-^{15}N PDSD, NCA, and NCO, can be exploited for resonance assignments of proteins and protein assemblies in the absence of ^{13}C labels, provided cryogenically cooled MAS NMR probes are used.

3.2.2. U-^{13}C,^{15}N-CA conical assembly

In addition to the case of low intrinsic sensitivity, there is another scenario where cryogenically cooled MAS NMR could potentially offer large benefits. This relates to high concentration samples of low stability, which require data collection as fast as possible. To mimic such conditions, we examined conical assembly of HIV-1 U-^{13}C,^{15}N-CA capsid protein, with 65 mg of isotopically labeled material packed into the MAS rotor. The resulting 1D and 2D spectra are shown in Fig. 5a–d. The CORD spectrum was collected with only 2 scans in 1.7 h, and exhibited a SNR of 114.7 for the 1st FID. This is a remarkably high value. Similarly, an outstanding-quality 2D NCACX spectrum was collected with 40 scans in 2.1 h, and SNR of 26 for the 1st FID was reached.

Likewise, the quality of the 3D NCACX and NCOCX data sets is equally high, both in terms of sensitivity and resolution (Fig. 6). It took 64 and 18.5 h to records the NCACX and NCOCX spectra, with SNRs for the 1st FIDs of 22.2 and 17.5, respectively. Using all these data sets, combined with the 2D CORD spectrum, we were able to derive backbone resonance assignments for a significant fraction of the CA residues in this assembly (Fig. 6).

3.3. Fibrils of prion proteins

3.3.1. Human Y145Stop PrP fibrils

Results that are in line with those described above for Kif5b/microtubule and HIV-1 CA assemblies were also obtained for U-^{13}C,^{15}N-labeled huPrP23-144 amyloid fibrils (Fig. 7). Specifically,

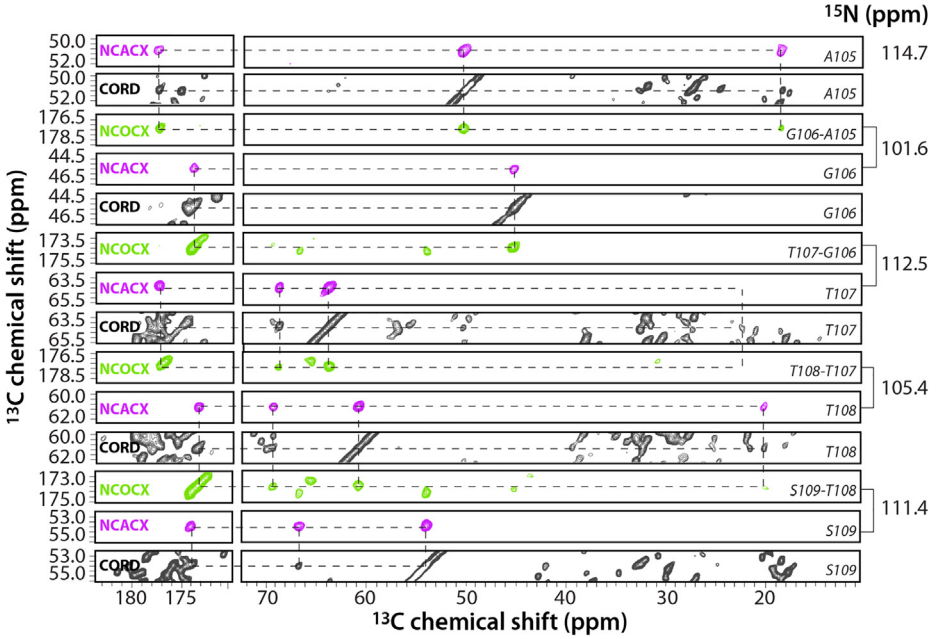

Fig. 6. Selected strips for residues A105-S109 in U-^{13}C,^{15}N-CA conical assembly from 2D CORD (black), 3D NCACX (magenta), and 3D NCOCX (green) spectra. The CORD spectrum was acquired with 16 scans per FID; the recycle delay was 2.5 s; the total experiment time was 11.4 h. The NCACX spectrum was acquired with 16 scans per FID, as a 1536 × 96 × 50 ($t_3 \times t_2 \times t_1$) complex matrix. The recycle delay was 3 s, and the total experiment time was 64 h. The NCOCX spectrum was acquired with 8 scans per FID, as 1536 × 64 × 52 ($t_3 \times t_2 \times t_1$) complex matrix. The recycle delay was 2.5 s, and the total experiment time was 18.5 h. (For interpretation of the references to color in this figure legend, the reader is referred to the web version of this article.)

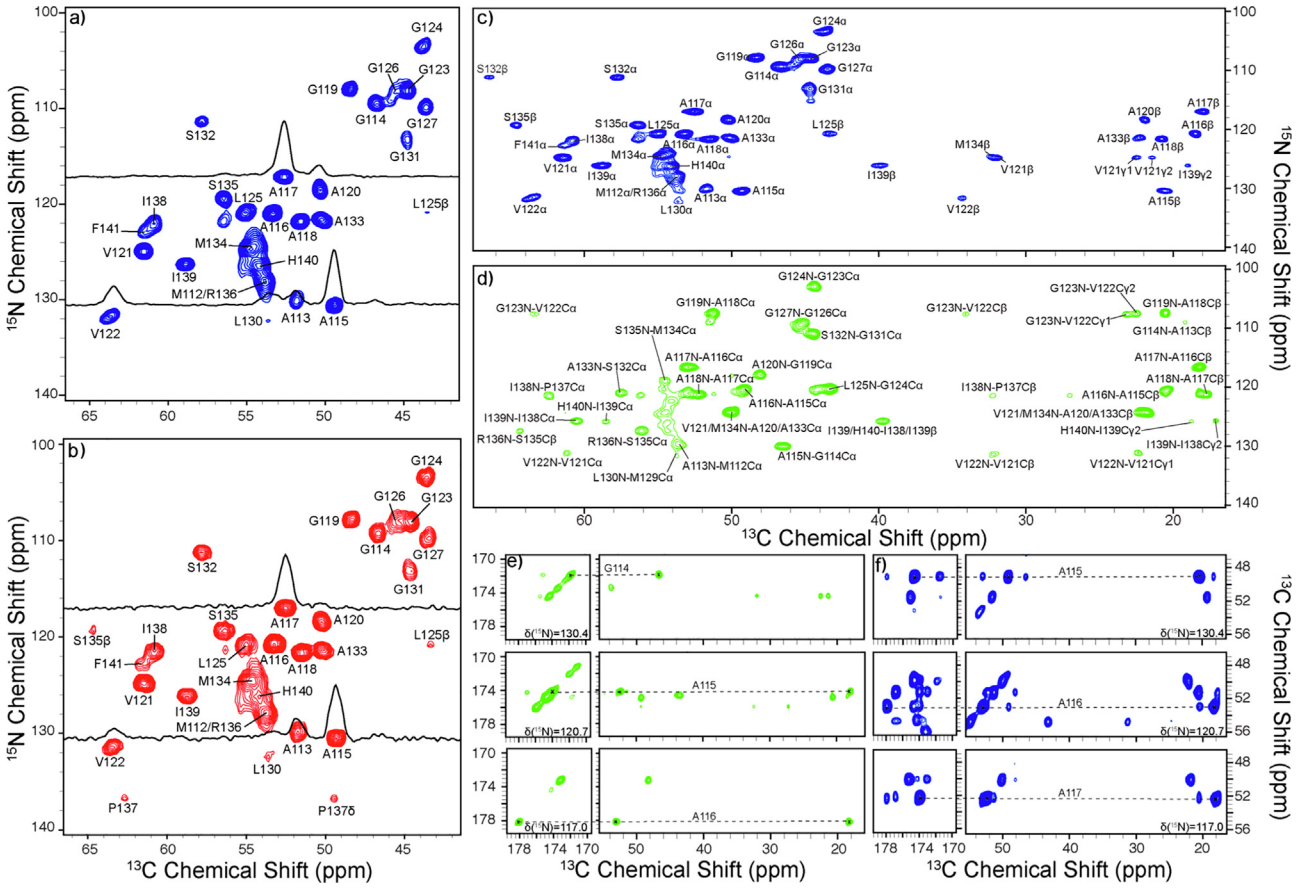

Fig. 7. 2D and 3D MAS NMR spectra of U-^{13}C,^{15}N huPrP23-144 fibrils recorded using the 3.2 mm CPMAS CryoProbe at 600 MHz and 13 kHz MAS rate. a) 2D NCA spectrum recorded as a 1024 × 47 ($t_2 \times t_1$) complex matrix with acquisition times of 15.3 ms (t_1) and 22.5 ms (t_2), 16 scans per row, 2.0 s recycle delay and a total measurement time of 50 min. b) A reference 2D NCA spectrum of U-^{13}C,^{15}N huPrP23-144 fibrils recorded with a total measurement time of 7 h using the 3.2 mm BioMAS probe at 500 MHz and 11.111 kHz MAS rate. The spectrum was collected with the same recycle delay and acquisition times in t_1 and t_2 as the 2D NCA spectrum in panel (a) and processed in identical manner. c) 2D N(CA)CX spectrum recorded with a DARR ^{13}C–^{13}C mixing time of 10 ms as a 681 × 57 ($t_2 \times t_1$) complex matrix with acquisition times of 18.7 ms (t_1) and 15.0 ms (t_2), 16 scans per row, 3.5 s recycle delay and a total measurement time of 1.8 h. d) 2D N(CO)CX spectrum recorded with a DARR ^{13}C–^{13}C mixing time of 50 ms as a 681 × 32 ($t_2 \times t_1$) complex matrix with acquisition times of 12.3 ms (t_1) and 15.0 ms (t_2), 64 scans per row, 3.5 s recycle delay and a total measurement time of 4 h. e) Representative planes corresponding to ^{15}N frequencies of residues A115, A116 and A117 from a 3D NCOCX spectrum recorded with a DARR ^{13}C–^{13}C mixing time of 50 ms as a 681 × 64 × 10 ($t_3 \times t_2 \times t_1$) complex matrix with acquisition times of 4.6 ms (t_1), 12.3 ms (t_2) and 15.0 ms (t_3), 16 scans per row, 3.5 s recycle delay and a total measurement time of 40 h. f) Representative planes corresponding to ^{15}N frequencies of residues A115, A116 and A117 from a 3D NCACX spectrum recorded with a DARR ^{13}C–^{13}C mixing time of 50 ms as a 388 × 40 × 16 ($t_3 \times t_2 \times t_1$) complex matrix with acquisition times of 6.2 ms (t_1), 6.2 ms (t_2) and 15.0 ms (t_3), 16 scans per row, 3.5 s recycle delay and a total measurement time of 40 h.

comparison of 2D NCA spectra acquired with comparable parameters using the 3.2 mm CPMAS CryoProbe at 600 MHz (Fig. 7a) and the 3.2 mm BioMAS room temperature probe at 500 MHz (Fig. 7b) reveals that data far superior in quality can be obtained in 50 min of measurement time with the CPMAS CryoProbe versus 7 h of measurement time with the BioMAS probe. For several well-resolved signals, corresponding to residues 115–118 located in the most rigid part of the amyloid fibril core [28,29], the average SNR is 102 ± 7 in the 50 min spectrum recorded using the CPMAS CryoProbe. Furthermore, a quantitative SNR comparison for the two experiments reveals a factor of ~4.5 sensitivity gain on average for the CPMAS CryoProbe, relative to the BioMAS probe after compensating for the different measurement times and static magnetic field strengths. In subsequent studies, the CPMAS CryoProbe was used to record high resolution and sensitivity 2D NCACX and NCOCX spectra for the PrP23-144 fibrils (Fig. 7c and d) with experiment times ranging from only ~1–4 h, which enabled nearly complete backbone and side-chain sequential resonance assignments. For completeness, we also recorded a pair of 3D NCACX and NCOCX spectra (Fig. 7e and f) with measurement times of 40 h per spectrum, which, if needed, could easily be reduced given the high SNR obtained for this particular fibril sample.

3.3.2. Fungal HET-s fibrils

Next, we examined the prion domain of the protein HET-s (218–289), forming amyloid fibrils associated with a very rigid amyloid core [30] and limited structural polymorphism. As such, the spectral quality of HET-s has been considered as a benchmark for insoluble and non-crystalline protein assemblies with a high content of β-sheet structure.

A comparison of 1D CP spectra of HET-s fibrils acquired at 14.1 T with the Efree probe and the CPMAS CryoProbe is shown in Fig. 8a and reveals a gain in sensitivity (~3) comparable to the microtubule assemblies and hPrP fibrils. 2D ^{13}C–^{13}C spectra are shown in Fig. 8b and c, with 1 scan for the CPMAS CryoProbe (Fig. 8b) and 16 scans for the Efree probe (Fig. 8c). The single-scan experiment on the CPMAS CryoProbe is sufficient to assess intra-residue ^{13}C–^{13}C correlations with high sensitivity and a short experimental time (~1.3 h). Several additional correlations in the C^{α}-C^{α} region are observed in the spectrum recorded with the

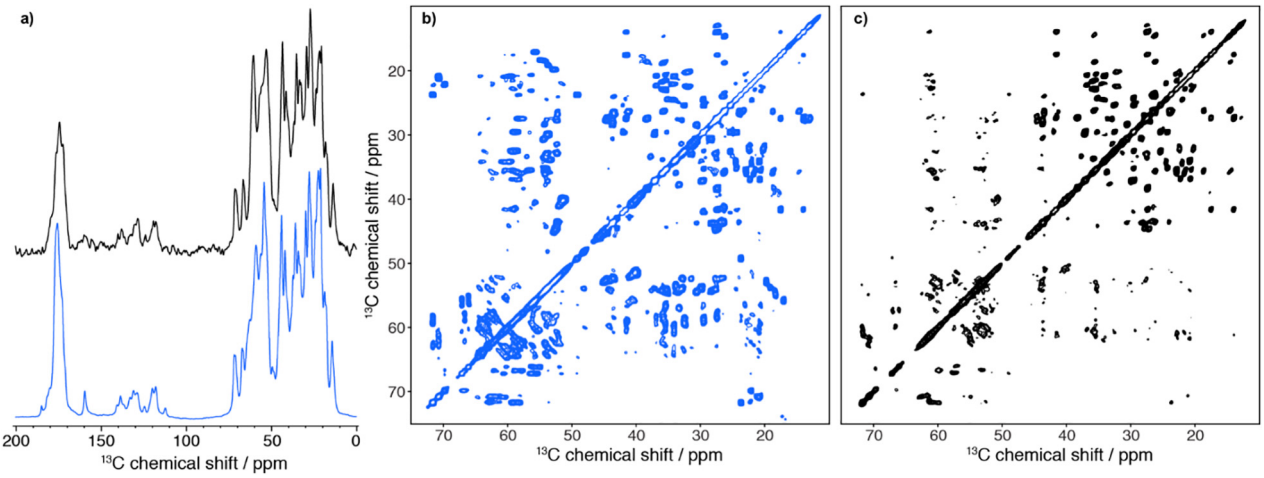

Fig. 8. a) 1D MAS CP spectra of HET-s (218–289) fibrils acquired with a single scan at 14.1 T with the 3.2 mm CPMAS CryoProbe (blue) and 3.2 mm EFree probe (black). (b and c) 2D PDSD spectra of HET-s (218–289) fibrils recorded at 14.1 T with the 3.2 mm CPMAS CryoProbe (b) and 3.2 mm EFree probe (c). The CC spectra were collected with 1 scan for the BioSolids CryoProb™e and 16 scans for the EFree probe, The recycle delays were respectively 3.5 and 2 s; the total experiment times were 1.3 and 10 h. The MAS frequency in both cases was 16 kHz. The estimated amount of HET-s (218–289) fibrils in the samples for experiments with the CPMAS CryoProbe and EFree probe was 21.4 and 10.0 mg. (For interpretation of the references to color in this figure legend, the reader is referred to the web version of this article.)

CPMAS CryoProbe, arising from sequential C^{α}-C^{α} connectivities observed with short mixing times.

4. Discussion

Here, we demonstrate for five different biological assemblies that significant gains in sensitivity can be achieved using the CPMAS CryoProbe. 3–4 fold intensity increases are seen in 1D CPMAS experiments, in line with the expectations based on the probe design. Surprisingly, however, 5–8 fold increases were observed in double CP-based experiments, possibly due to very high B_1 homogeneity of the CPMAS CryoProbe compared to a room temperature EFree probe. These enhancements translate into dramatic time savings in multidimensional experiments.

We selected several notoriously challenging systems for MAS NMR experiments: the Kif5b/MT assemblies containing less than 10% of isotopically labeled material, U-^{13}C,^{15}N-Kif5b, in the sample rendering most 3D heteronuclear correlation experiments with room temperature probes extremely challenging or prohibitive in required time. Using the CPMAS CryoProbe at 14.1 T, we acquired excellent quality 3D NCACX and NCOCX correlation spectra in a matter of 4.8 and 6.0 days, respectively. By comparison, the acquisition of the same data sets using an EFree probe at 20.0 T and 25% NUS required 15.8 and 19.3 days and resulted in inferior spectral quality.

Most rewardingly, it was possible to carry out 2D experiments on samples which contained only ^{15}N with carbons at natural abundance, as illustrated for the HIV-1 U-^{15}N-CA tubular assemblies. Indeed, it was possible to record high-quality 2D NCA/NCO data sets, which cannot be acquired with any available room temperature probe at any currently accessible magnetic field strength. More broadly, the set of experiments illustrated in Fig. 4 can provide resonance assignments for samples containing carbon at natural abundance, circumventing the necessity to introduce the more expensive ^{13}C labels.

Naturally, using the CPMAS CryoProbe is generally beneficial for all U-^{13}C,^{15}N-labeled protein samples, such as shown for HIV-1 CA protein tubular assemblies, fibrils of PrP and Het-s proteins. It is envisioned that the highest benefits of BioSolids cryogenic probes will be manifest in multi-user settings where quick turnaround is desirable, such as national or regional NMR facilities. Furthermore, such probes may find important uses in industrial applications, such as MAS NMR of biologics, where isotopic labels cannot be introduced readily but sample amounts are not a limiting factor.

Taken together, our results suggest that cryogenic probe technology for MAS NMR will open doors for atomic-level investigations of a wide variety of large and complex biological systems, including at natural isotopic abundance.

Declaration of Competing Interest

The authors declare that they have no known competing financial interests or personal relationships that could have appeared to influence the work reported in this paper.

Acknowledgment

This work is a contribution from the Pittsburgh Center for HIV Protein Interactions. A.M.G. and T.P. acknowledge the support of the National Institutes of Health, NIH Grant P50 AI150481, Technology Development Project 2. T.P. thanks the National Science Foundation, NSF CHE0959496 grant, for the acquisition of the 850 MHz NMR spectrometer and the NIGMS P30 GM110758 grant for the support of core instrumentation infrastructure at the University of Delaware. C.P.J. acknowledges support from the National Institutes of Health (R01GM094357, R01GM123743, RF1AG061797) and the National Science Foundation (MCB-1715174). A.Lo. acknowledges the European Research Council (2015-StG Weakinteract GA 63902). A.Le. thanks the Swiss National Science Foundation for early postdoc mobility project P2EZP2_184258. B.H. thanks the support by the CNRS Momentum.

Appendix A. Supplementary material

Supplementary data to this article can be found online at https://doi.org/10.1016/j.jmr.2019.106680.

References

[1] M.P. Rout, A. Sali, Principles for integrative structural biology studies, Cell 177 (2019) 1384–1403.
[2] C.M. Quinn, T. Polenova, Structural biology of supramolecular assemblies by magic-angle spinning NMR spectroscopy, Q. Rev. Biophys. 50 (2017) e1.
[3] C.M. Quinn, M. Wang, T. Polenova, NMR of macromolecular assemblies and machines at 1 GHz and beyond: new transformative opportunities for molecular structural biology, Methods Mol. Biol. 1688 (2018) 1–35.

[4] L.B. Andreas, K. Jaudzems, J. Stanek, D. Lalli, A. Bertarello, T. Le Marchand, D.C. D. Paepe, S. Kotelovica, I. Akopjana, B. Knott, et al., Structure of fully protonated proteins by proton-detected magic-angle spinning NMR, Proc. Natl. Acad. Sci. U. S. A. 113 (2016) 9187–9192.
[5] J. Stanek, L.B. Andreas, K. Jaudzems, D. Cala, D. Lalli, A. Bertarello, T. Schubeis, I. Akopjana, S. Kotelovica, K. Tars, et al., NMR spectroscopic assignment of backbone and side-chain protons in fully protonated proteins: microcrystals, sedimented assemblies, and amyloid fibrils, Angew. Chem.-Int. Edit. 55 (2016) 15504–15509.
[6] V. Agarwal, S. Penzel, K. Szekely, R. Cadalbert, E. Testori, A. Oss, J. Past, A. Samoson, M. Ernst, A. Bockmann, et al., De Novo 3D structure determination from sub-milligram protein samples by solid-state 100 kHz MAS NMR spectroscopy, Angew. Chem.-Int. Edit. 53 (2014) 12253–12256.
[7] S. Penzel, A.A. Smith, V. Agarwal, A. Hunkeler, M.-L. Org, A. Samoson, A. Böckmann, M. Ernst, B.H. Meier, Protein resonance assignment at MAS frequencies approaching 100 kHz: a quantitative comparison of J-coupling and dipolar-coupling-based transfer methods, J. Biomol. NMR 63 (2015) 165–186.
[8] S. Penzel, A. Oss, M.L. Org, A. Samoson, A. Bockmann, M. Ernst, B.H. Meier, Spinning faster: protein NMR at MAS frequencies up to 126 kHz, J. Biomol. NMR 73 (2019) 19–29.
[9] S. Yan, C. Guo, G. Hou, H. Zhang, X. Lu, J.C. Williams, T. Polenova, Atomic-resolution structure of the CAP-Gly domain of dynactin on polymeric microtubules determined by magic angle spinning NMR spectroscopy, Proc. Natl. Acad. Sci. USA 112 (2015) 14611–14616.
[10] J. Yehl, E. Kudryashova, E. Reisler, D. Kudryashov, T. Polenova, Structural analysis of human Cofilin 2/filamentous actin assemblies: atomic-resolution insights from magic angle spinning NMR spectroscopy, Sci. Rep. 7 (2017) 44506.
[11] S. Lange, W.T. Franks, N. Rajagopalan, K. Doring, M.A. Geiger, A. Linden, B.J. van Rossum, G. Kramer, B. Bukau, H. Oschkinat, Structural analysis of a signal peptide inside the ribosome tunnel by DNP MAS NMR, Sci. Adv. 2 (2016) e1600379.
[12] Y. Han, G.J. Hou, C.L. Suiter, J. Ahn, I.J.L. Byeon, A.S. Lipton, S. Burton, I. Hung, P. L. Gor'kov, Z.H. Gan, et al., Magic angle spinning NMR reveals sequence-dependent structural plasticity, dynamics, and the spacer peptide 1 conformation in HIV-1 capsid protein assemblies, J. Am. Chem. Soc. 135 (2013) 17793–17803.
[13] J.J. Helmus, K. Surewicz, P.S. Nadaud, W.K. Surewicz, C.P. Jaroniec, Molecular conformation and dynamics of the y145stop variant of human prion protein in amyloid fibrils, Proc. Natl. Acad. Sci. USA 105 (2008) 6284–6289.
[14] T. Theint, P.S. Nadaud, K. Surewicz, W.K. Surewicz, C.P. Jaroniec, ^{13}C and ^{15}N chemical shift assignments of mammalian y145stop prion protein amyloid fibrils, Biomol. NMR Assign. 11 (2017) 75–80.
[15] T. Theint, P.S. Nadaud, D. Aucoin, J.J. Helmus, S.P. Pondaven, K. Surewicz, W.K. Surewicz, C.P. Jaroniec, Species-dependent structural polymorphism of y145stop prion protein amyloid revealed by solid-state NMR spectroscopy, Nat. Commun. 8 (2017) 753.
[16] K.R. Thurber, R. Tycko, Measurement of sample temperatures under magic-angle spinning from the chemical shift and spin-lattice relaxation rate of ^{79}Br in KBr powder, J. Magn. Reson. 196 (2009) 84–87.
[17] J.A. Stringer, C.E. Bronnimann, C.G. Mullen, D.H. Zhou, S.A. Stellfox, Y. Li, E.H. Williams, C.M. Rienstra, Reduction of RF-induced sample heating with a scroll coil resonator structure for solid-state NMR probes, J. Magn. Reson. 173 (2005) 40–48.
[18] A. Bockmann, C. Gardiennet, R. Verel, A. Hunkeler, A. Loquet, G. Pintacuda, L. Emsley, B.H. Meier, A. Lesage, Characterization of different water pools in solid-state NMR protein samples, J. Biomol. NMR 45 (2009) 319–327.
[19] F. Delaglio, S. Grzesiek, G.W. Vuister, G. Zhu, J. Pfeifer, A. Bax, NMRPipe: a multidimensional spectral processing system based on UNIX pipes, J. Biomol. NMR 6 (1995) 277–293.
[20] T.D. Goddard, D.G. Kneller, SPARKY 3, University of California, San Francisco, 2004.
[21] J.J. Helmus, C.P. Jaroniec, Nmrglue: an open source python package for the analysis of multidimensional NMR data, J. Biomol. NMR 55 (2013) 355–367.
[22] S.P. Skinner, R.H. Fogh, W. Boucher, T.J. Ragan, L.G. Mureddu, G.W. Vuister, CcpNmr AnalysisAssign: a flexible platform for integrated NMR analysis, J. Biomol. NMR 66 (2016) 111–124.
[23] M.R. Palmer, C.L. Suiter, G.E. Henry, J. Rovnyak, J.C. Hoch, T. Polenova, D. Rovnyak, Sensitivity of nonuniform sampling NMR, J. Phys. Chem. B 119 (2015) 6502–6515.
[24] S. Paramasivam, C.L. Suiter, G. Hou, S. Sun, M. Palmer, J.C. Hoch, D. Rovnyak, T. Polenova, Enhanced sensitivity by nonuniform sampling enables multidimensional MAS NMR spectroscopy of protein assemblies, J. Phys. Chem. B 116 (2012) 7416–7427.
[25] C.L. Suiter, S. Paramasivam, G. Hou, S. Sun, D. Rice, J.C. Hoch, D. Rovnyak, T. Polenova, Sensitivity gains, linearity, and spectral reproducibility in nonuniformly sampled multidimensional MAS NMR spectra of high dynamic range, J. Biomol. NMR 59 (2014) 57–73.
[26] M. Lu, G. Hou, H. Zhang, C.L. Suiter, J. Ahn, I.J. Byeon, J.R. Perilla, C.J. Langmead, I. Hung, P.L. Gor'kov, et al., Dynamic allostery governs cyclophilin A-HIV capsid interplay, Proc. Natl. Acad. Sci. USA 112 (2015) 14617–14622.
[27] G. Bodenhausen, R. Freeman, G.A. Morris, A simple pulse sequence for selective excitation in Fourier transform NMR, J. Magn. Reson. 23 (1976) 171–175.
[28] J.J. Helmus, K. Surewicz, W.K. Surewicz, C.P. Jaroniec, Conformational flexibility of y145stop human prion protein amyloid fibrils probed by solid-state nuclear magnetic resonance spectroscopy, J. Am. Chem. Soc. 132 (2010) 2393–2403.
[29] M.D. Shannon, T. Theint, D. Mukhopadhyay, K. Surewicz, W.K. Surewicz, D. Marion, P. Schanda, C.P. Jaroniec, Conformational dynamics in the core of human y145stop prion protein amyloid probed by relaxation dispersion NMR, Chemphyschem 20 (2019) 311–317.
[30] C. Wasmer, A. Lange, H. Van Melckebeke, A.B. Siemer, R. Riek, B.H. Meier, Amyloid fibrils of the HET-s(218–289) prion form a beta solenoid with a triangular hydrophobic core, Science 319 (2008) 1523–1526.